Article

Current Biology

A Plausible Microtubule-Based Mechanism for Cell Division Orientation in Plant Embryogenesis

Graphical Abstract

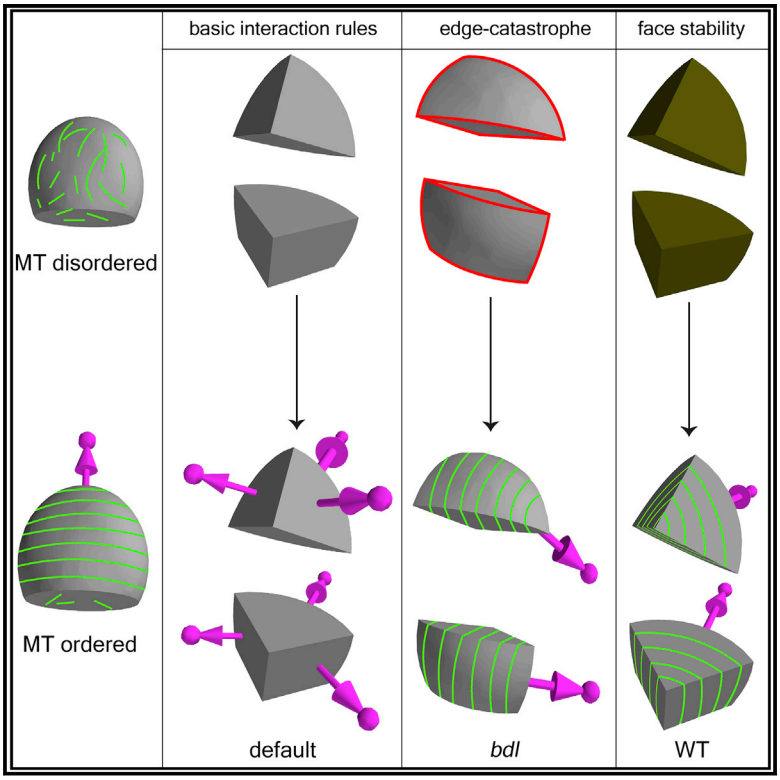

Highlights

- Cortical microtubule dynamics is simulated on experimentally extracted cell shapes
- Cell geometry, edge effects, and developmental cues affect microtubule dynamics
- Cortical microtubule array orientation can predict division planes in plant embryos
- Predictions match observations in wild-type and two developmental mutants

Authors

Bandan Chakrabortty, Viola Willemsen, Thijs de Zeeuw, Che-Yang Liao, Dolf Weijers, Bela Mulder, Ben Scheres

Correspondence

mulder@amolf.nl (B.M.), ben.scheres@wur.nl (B.S.)

In Brief

Chakrabortty et al. show that a computational model for dynamic self-organization of cortical microtubules on experimentally extracted cell shapes provides a plausible molecular mechanism for division plane orientation in the first four divisions of early stage *A. thaliana* embryos, in WT as well as two developmental mutants *bodenlos* and *clasp*.

Chakrabortty et al., 2018, Current Biology *28*, 3031–3043
October 8, 2018
https://doi.org/10.1016/j.cub.2018.07.025

CellPress

Current Biology
Article

A Plausible Microtubule-Based Mechanism for Cell Division Orientation in Plant Embryogenesis

Bandan Chakrabortty,[1,2] Viola Willemsen,[1,5] Thijs de Zeeuw,[4,5] Che-Yang Liao,[4] Dolf Weijers,[4] Bela Mulder,[2,3,*] and Ben Scheres[1,6,*]
[1]Plant Developmental Biology, Wageningen University, Wageningen 6708 PB, the Netherlands
[2]Theory of Biomolecular Matter, Institute AMOLF, Science Park 104, 1098 XG Amsterdam, the Netherlands
[3]Cell Biology, Wageningen University, Wageningen 6708 PB, the Netherlands
[4]Laboratory of Biochemistry, Wageningen University, Stippeneng 4, 6708 WE Wageningen, the Netherlands
[5]These authors contributed equally
[6]Lead Contact
*Correspondence: mulder@amolf.nl (B.M.), ben.scheres@wur.nl (B.S.)
https://doi.org/10.1016/j.cub.2018.07.025

SUMMARY

Oriented cell divisions are significant in plant morphogenesis because plant cells are embedded in cell walls and cannot relocate. Cell divisions follow various regular orientations, but the underlying mechanisms have not been clarified. We propose that cell-shape-dependent self-organization of cortical microtubule arrays is able to provide a mechanism for determining planes of early tissue-generating divisions and may form the basis for robust control of cell division orientation in the embryo. To show this, we simulate microtubules on actual cell surface shapes, from which we derive a minimal set of three rules for proper array orientation. The first rule captures the effects of cell shape alone on microtubule organization, the second rule describes the regulation of microtubule stability at cell edges, and the third rule includes the differential effect of auxin on local microtubule stability. These rules generate early embryonic division plane orientations and potentially offer a framework for understanding patterned cell divisions in plant morphogenesis.

INTRODUCTION

Plant cell division patterns show striking regularities. A prime example is the early-stage embryo in *Arabidopsis* [1–3], which starting from the single-cell stage undergoes a few rounds of remarkably robust and geometrically precise internal divisions, setting the stage for further development through differentiation and growth. For already more than a century, these regularities have spurred the formulation of heuristic geometric rules for oriented cell divisions. These rules relate the selection of division planes, e.g., to the principal direction of growth, geometric relations to existing cell walls and the nucleus, or minimum cell surface energy [4–9]. With the advent of modern cell biology, however, division plane orientation in plants has been connected with the orientation of the ordered ensemble of microtubules (MTs) associated with the plasma membrane, the cortical microtubule array (CMA) [10, 11]. Shortly before cell division, the cortical MTs, while keeping their net orientation, become spatially restricted to a plane that is closely associated with the nucleus, forming the so-called pre-prophase band (PPB). The orientation of the PPB and, by extension, that of the CMA is an indicator of cell division orientation [12, 13]. Some variability between PPB and cell plate orientation may occur (e.g., [14]), and recent evidence suggests that the PPB is not strictly required for division plane orientation [15], but nevertheless the link of cell division plane to CMA orientation is maintained. The question of how the CMA is organized is therefore of prime importance to understanding division plane orientation.

Here, we address this question in the early *Arabidopsis* embryo. Apart from the intrinsic biological interest of the tissue-separating (“formative”) cell divisions that occur in this system, it provides a unique, well-defined, and yet highly non-trivial “laboratory” for studying the interplay between the molecular mechanisms driving CMA organization and the developmental context. This holds a fortiori, as previous analysis of *Arabidopsis* embryogenesis surprisingly shows that auxin-insensitive embryos misexpressing the *bodenlos* (*bdl*) protein do divide consistent with proposed geometric rules, whereas wild-type (WT) divisions seem to require additional control [1], possibly through auxin-mediated CMA regulation. This indicates the need to elucidate to what extent the geometrical rules are in fact consistent with concrete molecular mechanisms.

There is a broad consensus that orientational ordering in the CMA is the collective outcome of the local effects of “collisions” between MTs driven by their dynamical instability mechanism [16]. Moreover, there is evidence gleaned from root epidermis cells that specific geometric features, such as sharps edges between relatively flat cell faces, can influence the orientation of the CMA by effectively blocking the passage of MTs from one cell face to the other and that this effect is possibly modulated by microtubule-associated protein (MAP) CLASP [17]. However, we as yet lack a full understanding of how cell shape in general impacts CMA organization. This is especially salient in the early *Arabidopsis* embryo, which, in its first 4 division cycles, displays a gamut of cell shapes, ranging from almost spherical to halves of spherical wedges with a sharp opening angle. Recently, tensile stress has also been shown to influence CMA orientation [18], leading to the proposal of a new general rule for division

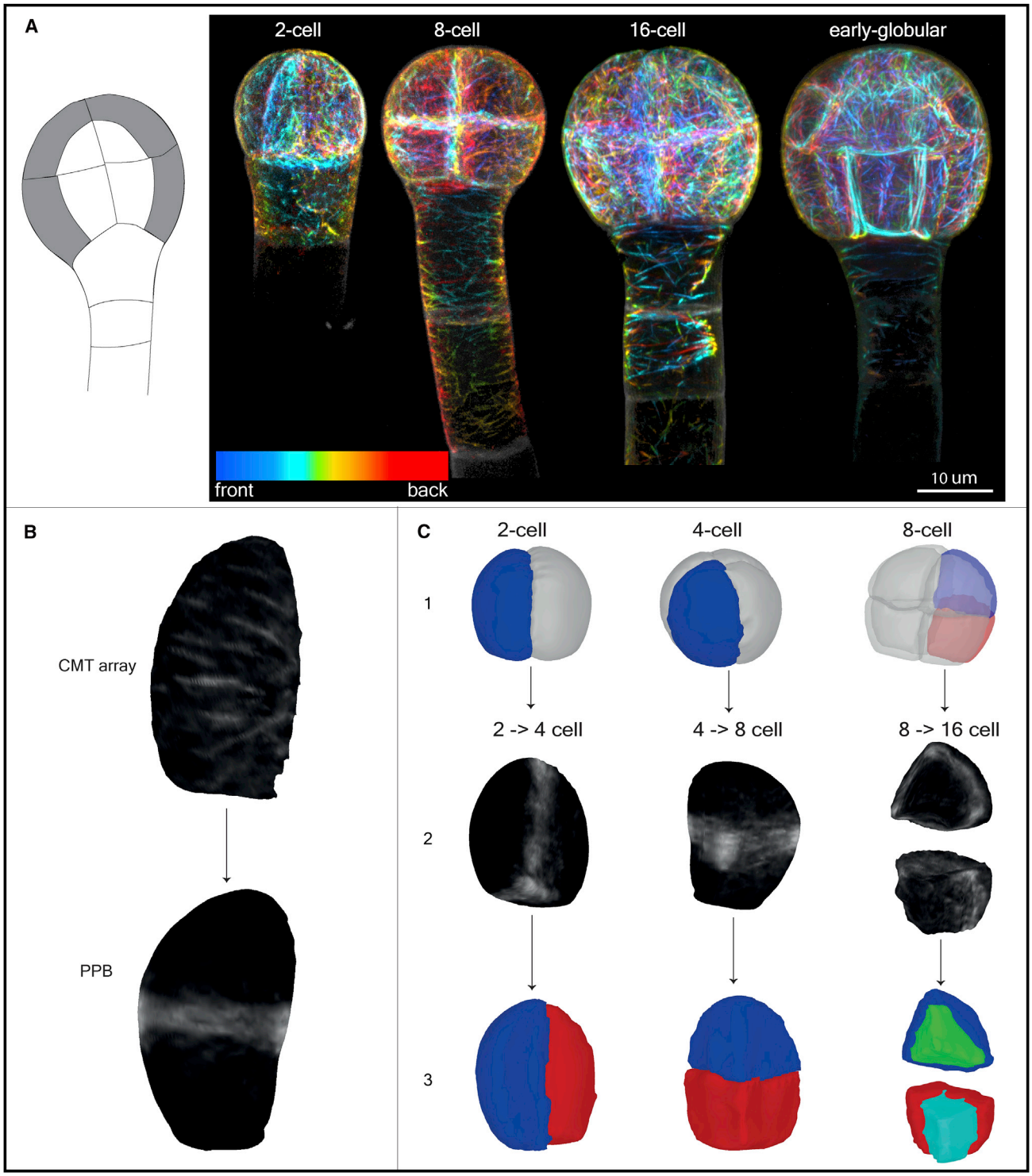

Figure 1. Experimental Visualization of CMA and PPB during *Arabidopsis* Early Embryonic Development

(A) Characteristic divisions lead to the formation of inner and outer tissue layers (left); maximum projection of depth-coded stacks of MTs visualized using a pWOX2::TUA6-GFP reporter line shows an ordered orientation of MT array (right). The look-up table shows color values corresponding to the depth of the image in the z-dimension.

(B) Sequential imaging of cortical MTs and the SR2200 membrane stain allows for extraction of cell shapes for separate embryonic cells. Projection of cortical MT signal on extracted cell shapes shows orientation of CMA that predicts the orientation of PPB (7 cells were analyzed; note that the images are taken from different cells in the same embryo, not from live imaging the same cell over time).

(legend continued on next page)

plane orientation along the direction of maximal wall tension [14]. However, to date, the molecular mechanism by which MTs "sense" the direction of wall tension remains elusive, although the activity of the MT-severing protein katanin appears to be implicated [19]. Finally, as cortical MTs co-align with cellulose microfibrils, growing cells exhibit a complex interplay between CMA orientation, the deposition of microfibrils in the cell wall, and growth [20, 21], so that growth by itself could influence division plane orientation, potentially underpinning one of the phenomenological rules [22].

Here, we utilize a recently developed computational framework that simulates the dynamics of MT ordering on realistic cell shapes [23]. We specifically focused on the impact of shape in a geometrical sense, including the described edge effects, on the collective dynamics of MTs that lead a global orientation of the CMA. This provides a clearly defined default model to which other effects may be added incrementally. As it is at present infeasible to directly measure or predict stress patterns in the embryo, and in the absence of a concrete molecular mechanism to implement the feedback of tension on MT dynamics, we parsimoniously chose to disregard these effects at this stage. Finally, as only a very limited amount of volumetric growth occurs during the considered embryonic developmental phase, potential growth-related effects were also ignored.

Combining our *in silico* results with high-resolution visualization of both cell outline and cortical MTs in WT *Arabidopsis* embryos and selected mutants enabled us to show that hitherto unanticipated constraints due to cell shape alone, in combination with cell edge-catastrophe protection and auxin-mediated MT stability, can already provide a sufficient explanation for cell division patterns in 1- to 16-cell stage embryos. Thus, our minimal MT-based molecular statistical mechanism correctly predicts division plane orientations, recapitulates many of the proposed geometric rules, and establishes a basis for specific experimental validations and the incorporation of additional mechanisms when necessary in the future.

RESULTS

First Principle-Based MT Modeling on Realistic Cell Shapes

Our approach for understanding rules of cell division in cells that undergo formative cell divisions was to model cortical MT dynamics during the first four division cycles in the *Arabidopsis* embryo proper, which have been documented in detail [1, 24–26]. These characteristic divisions lead to the formation of inner and outer tissue layers (Figure 1A, left). Our starting assumption was that embryonic cells, like most cell types previously considered, have a regular CMA orientation that predicts the orientation of cell division. To test this assumption, we utilized an optimized imaging methodology for high-resolution 3D imaging of the CMA, which preserves MT orientation throughout the different stages of *Arabidopsis* embryogenesis [27]. We expressed TUA6-GFP from the embryo-specific *WUSCHEL-RELATED HOMEOBOX 2* (*WOX2*) promoter. Maximum projections of high-resolution z stacks reveal the overall topology of the MT array, including the CMA, for embryos from the 1-cell stage to globular stage (Figure 1A, right). Cell segmentation allowed the extraction of individual cell surfaces for the different embryonic cells. Analysis of cortical MT signals projected on these extracted cell surfaces shows the ordered orientation of CMA on individual cells. The CMAs collapse to form PPB structures [28], and we found this to likely also be the case in embryos (Figure 1B), thus correctly predicting future division plane orientation (Figure 1C). Our observations validated the early embryo as a suitable model system to investigate how cortical MT ordering is established in cells with varying geometries.

To enable the exploration of a number of factors that, given observations in other cell types, are likely to govern CMA orientation in the early embryo, we designed a computational framework to simulate the key properties of MT dynamics on arbitrary shaped cellular surfaces. CMAs in animal cells have been shown to be sensitive to cell shape [29]. Therefore, we used the actual embryonic cell shapes obtained by segmenting high-resolution confocal images of fluorescently stained *Arabidopsis* embryos to extract cell surfaces, approximated through fine-grained triangulation (Figure 2A). To simulate MT dynamics on individual planar triangles, we adapted a previously developed event-driven algorithm [31, 32] that implements all key MT properties with biophysical significance, such as nucleation and dynamic instability [33]. In the latter mechanism, MTs alternate between states of steady growth or shrinkage, stochastically switching between these states at constant rates in events termed *catastrophes* and *rescues*, respectively. We also encoded three possible results from MT-MT collisions that have been observed [16], *zippering*, in which an impinging growing MT bends and continues growing along an obstructing MT; *crossover*, in which an impinging MT simply passes over an obstructing MT; and *induced-catastrophe*, in which the impinging MT switches to a shrinking state and retreats from the obstructing MT (Figure 2B). Additional factors are known to influence MT dynamics, most notably directional nucleation from existing MTs [34] and severing by katanin [19, 35]. At present, however, data are lacking to what extent these factors play a role in the early embryo. Also, previous modeling work has shown that these additional effects mainly modify the range of parameters for which ordered arrays develop spontaneously but have less impact on the nature of the ordered state per se [35–37]. They are therefore not expected to influence the results we present here, which involve the effect cell geometry and other developmental factors has on the global orientation of an otherwise spontaneously aligned MT array. For simplicity's sake, we therefore choose to omit these features at this stage but stress that they are all implemented in our simulation framework [35, 36]. Likewise, MTs that are nucleated in the bulk cytosol but become entrained to the cortex by binding to the cell membrane (see, e.g., [38])

(C) PPB predicts the location and orientation of the division plane: (1) representative single cell from 2-cell stage and 4-cell stage embryo and representative single cell from upper tier and lower tier of 8-cell stage embryo are highlighted; (2) projection of PPB on the corresponding cell templates during 2- to 4-cell stage (3 cells were analyzed), 4- to 8-cell stage (5 cells were analyzed), and 8- to 16-cell stage (5 cells were analyzed) transitions; and (3) pair of daughter cells during 2- to 4-, 4- to 8-, and 8- to 16-cell stage transitions. Figures S1A–S1C show the cortical localization of MTs.

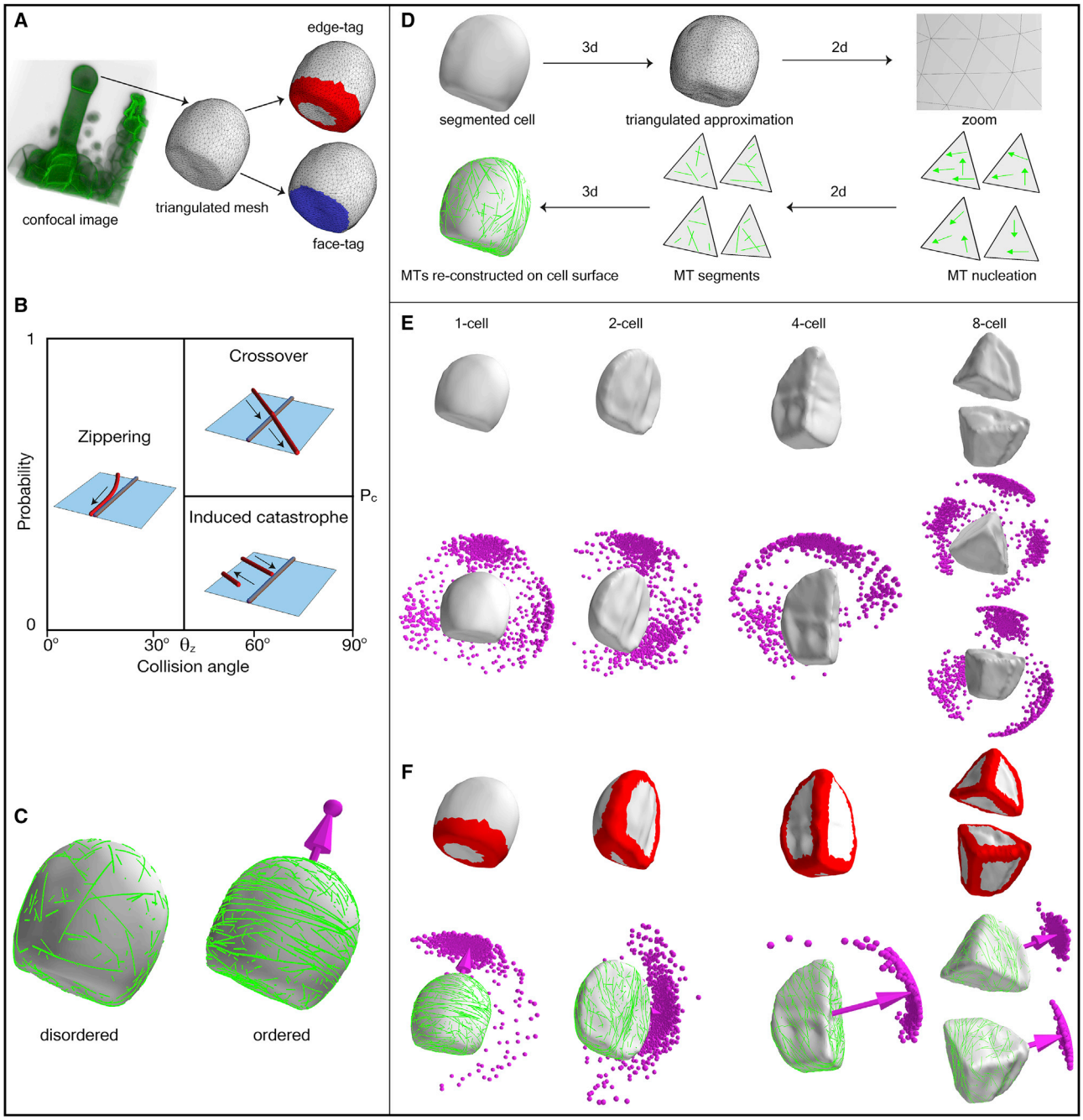

Figure 2. MT Modeling on *Arabidopsis* Early Embryonic Cell Templates

(A) The confocal image of embryonic 1-cell shape is extracted as a triangulated surface mesh via image segmentation software MorphoGraphX [30]. The edge of the mesh is tagged (red color) by assigning all triangles belonging to this edge with a unique edge-tag index. The flat-bottom face (faint blue) and the curved-top face (faint gray) are tagged by assigning all their triangles with a unique face-tag index. Edge tags and face tags are used for simulation implementation of edge-catastrophe and face-specific MT stabilization.

(B) Basic MT-MT interactions. Two-dimensional attachment of MTs to cell cortex allows MTs to interact with each other via collisions. Shallow angles ($\leq 40^{\circ}$) of collision lead to *zippering*, and steeper angles ($\geq 40^{\circ}$) of collision lead to *crossover* or *induced-catastrophe*.

(C) Order parameter to quantify the degree of MT order and array orientation. A disordered state results in $Q^{(2)} \sim 0$ without formation of MT array. An ordered state indicates the formation of MT array with significant degree of MT order, $Q^{(2)} \sim 1$. Perpendicular to the MT array, a vector $(\vec{\Omega})$ is defined that quantifies the orientation of the MT array. The tip of this vector will be used to represent the MT array orientation.

(D) A schematic overview of the simulation approach, where geometrically correct propagation of growing MT ends between the neighboring triangles lead to the reconstruction of MT dynamics on the cell surfaces.

(legend continued on next page)

effectively only increase the nucleation rate. Parsimony therefore led us to omit these features here. The simulations on individual triangles are linked together by ensuring that the trajectories of MTs crossing from a triangle to a neighboring one are propagated in a manner consistent with the 3D geometry of the cell surface, as illustrated in Figure 2D. The technical details of our simulation procedure, its validation against known results, and illustrative background results on the interplay between geometry and CMA organization on simple shapes are more fully explained in a recently published method paper [23].

Earlier work has shown that all parameters of individual MT behavior, excluding collision parameters, can be absorbed in a single dimensionless control parameter (G) that controls the frequency of MT interactions [37, 39],

$$G = \left(\frac{2(v_+ - v^{tm})(v_- + v^{tm})}{r_n(v_+ + v_-)}\right)^{1/3}\left(\frac{r_r}{(v_- + v^{tm})} - \frac{r_c}{(v_+ - v^{tm})}\right),$$

where v_+, v_-, and v^{tm} are the growth, shrinkage, and minus-end treadmilling speeds of the MTs, r_c and r_r the catastrophe- and rescue rates, and r_n the rate of MT nucleations per unit of cell surface area. By convention, the sign of G is chosen such that $G < 0$ when the MTs are in the biologically relevant bounded growth regime. If G increases beyond a threshold value, the interacting cortical MTs will spontaneously form an ordered array. G can be increased (i.e., brought closer to 0) in several ways. For example, the higher nucleation rate r_n, the more MTs are present, which increases the frequency of collisions in the cortex. Likewise, decreasing the catastrophe rate r_c makes the MTs longer on average, which makes them more likely to interact through collisions. As the value of G can be freely chosen on each triangle, we are able to modulate MT behavior on selected areas of the cell surface, corresponding to biologically controlled effects, e.g., developmentally distinct cell faces and/or highly curved edge regions between cell faces.

To read out the order of the steady-state CMA, we employed a tensorial order parameter $\mathbf{Q}^{(2)}$ (for details of its definition, see [23]), whose absolutely smallest eigenvalue $Q^{(2)}$ characterizes the degree of ordering: $Q^{(2)} \sim 0$ when MT orientation is random and $Q^{(2)} \sim 1$ when MTs are almost aligned. The normalized eigenvector $\widehat{\Omega}$ associated with the eigenvalue $Q^{(2)}$ characterizes the global orientation of the MT array. Its direction is perpendicular to the plane in which on average the MTs are pointing, i.e., if the MTs form a dense band around the "equator" of a cell, $\widehat{\Omega}$ will point to one of the "poles." In all simulation images, $\widehat{\Omega}$ is represented by a dot marking the end point of the vector (Figure 2C).

Shape and Edge-Catastrophe Can Explain Early Embryo Cell Division Patterns in an Auxin Response Mutant

We performed ≈1,000 stochastically independent simulations of MT dynamics per cell on cell surfaces extracted from WT embryos from 1- to 8-cell stage, ensuring throughout that a steady state was reached. The resulting CMAs displayed a diverse, but not randomly distributed, orientation (Figure 2E; quantification in Figure 7A). Thus, cell shape significantly impacted but could not uniquely specify the orientation of the CMAs on a given cell template. It has been reported that cell edges may hinder the propagation of MTs in plant cells depending on their degree of curvature [17]. We were curious whether this reported property of MT behavior could further reduce the diversity of CMA orientations in our simulations. We implemented a local enhanced catastrophe in those cell edges that have high curvature. In the various WT cells, this implementation robustly reduced the possible CMA orientations to a single sharply defined cluster for each cell stage (Figure 2F). However, the resultant inferred division patterns were non-WT and instead appeared to match those of the auxin-insensitive embryos ectopically expressing *bdl* protein (RPS5A>>bdl) [1]. Moreover, the simulations predicted a preference for slightly oblique division at the 4-cell stage in auxin-insensitive embryos, hitherto not described. We experimentally verified this preference of oblique division for 4- to 8-cell stage transition in RPS5A>>bdl embryos as well as their aberrant divisions in 8- to 16-cell stage transition [1] (Figure S2). Note that, at the 1- to 2-cell transition, all simulations yielded horizontal divisions, whereas only 18% of the original *bdl* mutant (non-overexpressed) divides in this direction [40]. To exclude that the mapping to *bdl* division patterns was a coincidental effect of using WT cell templates, we extracted cell templates from 4- to 16-cell stages RPS5A>>bdl embryos, reconstructed progenitor 2- to 8-cell stage cell surfaces by merging corresponding daughter cell pairs, and ran simulations on these reconstructed "mother cells" (Figure 3A). The steady-state CMA orientation in all these simulations correctly predicted the division plane, confirming that shape effects and edge-catastrophe were sufficient to explain *bdl* divisions between 2- and 16-cell stages (Figure 3B). For a quantification of the predicted division plane angles with respect to the basal plane compared to experimentally measured values, see Figure 7B.

Face Stability and Edge-Catastrophe Reduction Explain WT Early Embryo Cell Division Patterns

The highly characteristic WT division pattern at the 8- to 16-cell stage transition that separates inner and outer cell layers did not follow the rules based on cell shape and edge-catastrophe only. To search for an additional rule that might explain the WT division pattern, we first focused on the divisions between 2- and 16-cell stages, which were correctly predicted in *bdl* mutant cells. We asked whether the observed defects with respect to WT were associated with aberrant CMA formation. In *RPS5A>bdl* embryos, the cytosolic (non-polymerized) TUA6:GFP fraction was significantly higher, suggesting that MTs were more often depolymerized compared to WT. This indicates that reduced auxin signaling affects MT polymerization or stability in embryo cells (Figure S1D). We implemented this observation in our simulations by allowing auxin-dependent, cell-face-specific changes in the G parameter, leading to locally

(E and F) Simulated orientation of MT array on 1- to 8-cell stage WT cell templates: (E) default cell shapes, which showed a diverse, but not randomly distributed, MT array orientation, and (F) with edge-catastrophe in MT dynamics, which showed one unique cluster of MT array orientation in each cell stage. Simulations were performed for ≈1,000 independent configurations of stochastic MT dynamics. The arrow vectors represent mean orientation of the associated MT array. See also Figure S3.

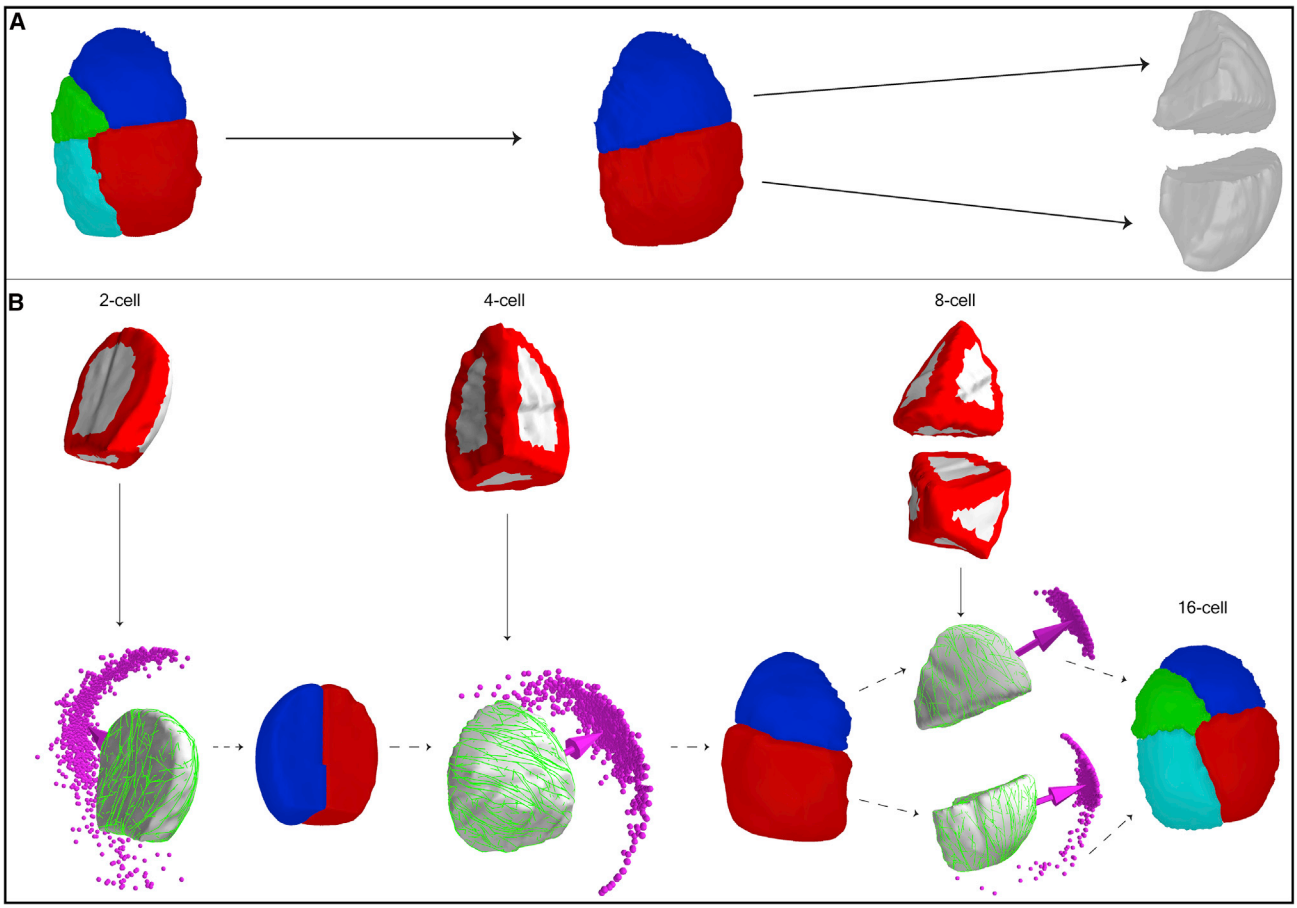

Figure 3. Recapitulation of *bdl* Division Patterns in *Arabidopsis* Early Embryonic Development

(A) Reconstruction of mother cell by merging the corresponding daughter cell pair. In this example, the daughter pair of both upper and lower tier of *Arabidopsis bdl* 16-cell template was merged to reconstruct the corresponding mother 8-cell template. Such re-created mother cells were separated out for simulating MT dynamics.

(B) Simulated MT arrays on 2- to 8-cell stage of *bdl* cell template, which were reconstructed by merging the corresponding daughter cell pair of the next cell stage. Simulations were performed with edge-catastrophe, yielding one unique cluster of MT array orientation in each cell stage, which correctly predicted the corresponding *bdl* division plane orientation. Cell edges are colored red to indicate that, in simulation, MTs were subjected to edge-catastrophes.

See also Figures S2, S3, and S7.

enhanced average MT stability (Figure S3). The resulting simulations therefore implemented, next to the basic rules for MT dynamics, effects of two biological control parameters: auxin-regulated face stability (Figure 4A) and edge-catastrophe. We investigated multiple combinations of the strength of these two effects yielding different behavioral regimes. A complete match with WT division patterns (Figure 4B; quantification in Figures 7C and S4) was obtained by simulating MT dynamics on "original" or "reconstructed mother" 2- to 8-cell stage cell templates under the following adaptations of our initial rules: (1) enhanced cell face stability that is strongest in recent division faces and (2) reduced edge-catastrophe (for simulation parameters, see Figure S3). These specific rules conceivably result from concrete molecular processes. First, auxin-mediated enhanced face stability could be transiently established at each new division site. Second, edge-catastrophe could be reduced, for example, by the activity of proteins that stabilize bending MTs [17].

As an initial test of the requirement of edge-catastrophe reduction for obtaining correctly oriented CMAs between 2- and 16-cell stages in WT, we analyzed embryos homozygous for two different mutations in the *CLASP* gene, reported to influence MT edge-catastrophe [17]. To support our assumption that edge-catastrophe is regulated in WT embryos by CLASP, its mutations should affect division plane orientation in a manner predicted by our simulations. Indeed, in both mutant alleles, division orientations were severely skewed compared to WT (Figure 5A for 4- to 8-cell stage; Figure S5 for all 1- to 16-cell stage). To test whether we could correctly predict division planes in *clasp* mutant embryos, we first focused on the resulting sister cells of 4- to 8-cell stage transition in the *clasp* mutant to reconstruct mother cell and then simulated CMA orientation on the resulting cell shape. We used WT settings for auxin-mediated face stability, assumed to be unaffected, but introduced increased edge-catastrophes to simulate loss of CLASP. Under these conditions, the

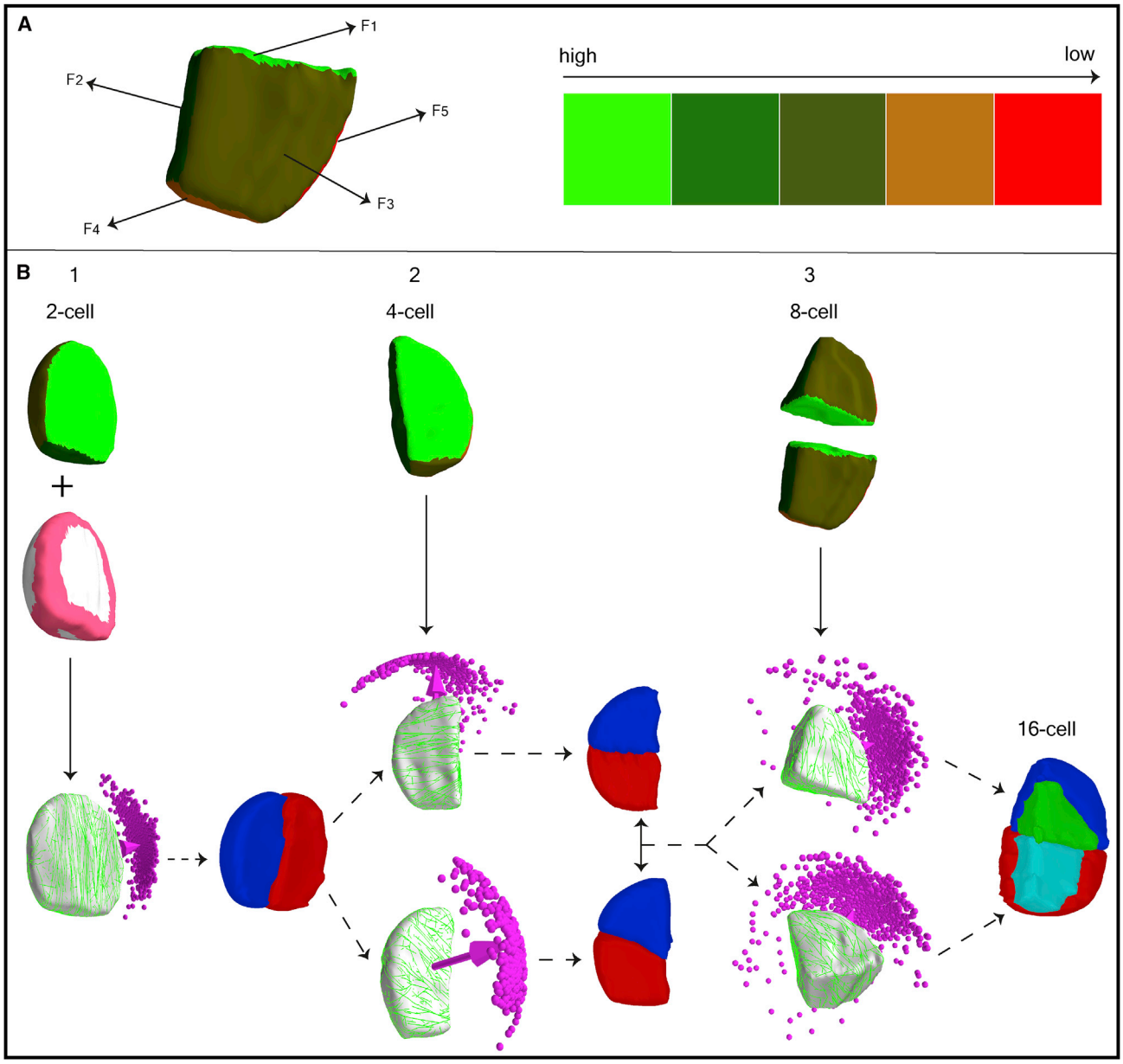

Figure 4. WT Division Pattern in *Arabidopsis* Early Embryonic Development

(A) Developmental age of cell faces $F_5 > F_4 > F_3 > F_2 > F_1$ as depicted by the color scale. MT dynamic catastrophe rate increases with developmental age, yielding a corresponding decrease in average MT length, i.e., lower MT stability.

(B) Simulated orientation of MT array on WT cell templates taken from different cell stages: (1) 2-cell stage with reduced edge-catastrophe in MT dynamics and enhanced MT stabilization at developmentally new cell faces, resulting in one unique cluster of MT array orientation correctly predicting the WT division plane orientation; (2) 4-cell stage without edge-catastrophe in MT dynamics and enhanced MT stabilization at developmentally new cell faces, resulting in two clusters of MT array orientation correctly predicting the two observed phenotypes of WT division plane orientation; and (3) 8-cell stage without edge-catastrophe in MT dynamics and enhanced MT stabilization at developmentally new cell faces, resulting in one unique cluster of MT array orientation for both upper and lower tier cells correctly predicting the WT division plane orientation.

See also Figures S1D, S3, and S4.

observed CMA orientations indeed robustly predicted the observed division planes in the *clasp* mutant (Figure 5B; quantification in Figure 7D). In conclusion, the model assumptions that result in WT division pattern also yield, *mutatis mutandis*, the aberrant division pattern of *clasp* at the critical 4- and 8-cell stage transition.

Tuning of Face Stability and Edge-Catastrophe Allows Prediction of All Early Embryo Cell Division Patterns

Our model so far predicted correct WT division patterns between the 2- and 16-cell stage when both auxin-mediated face stability and CLASP-mediated edge-catastrophe reduction are implemented. This same implementation of the model also

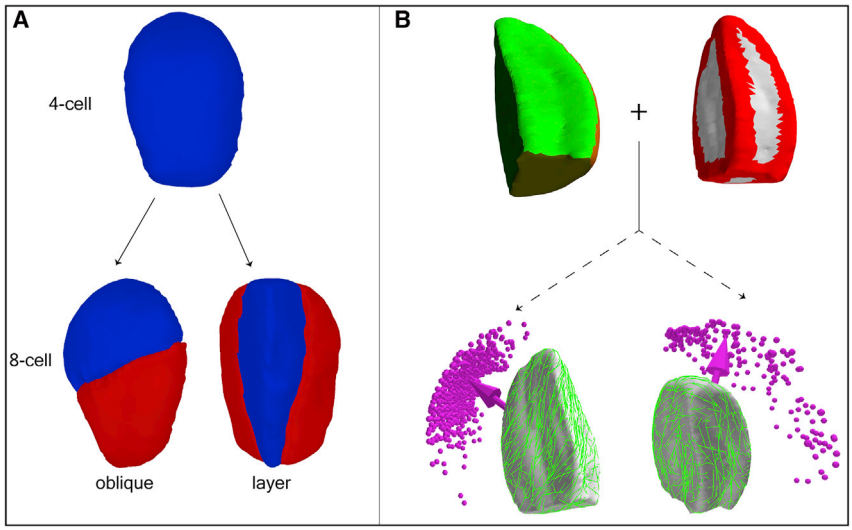

Figure 5. Simulating *clasp* Mutant Division Patterns in *Arabidopsis* Early Embryonic Development

(A) Representative *clasp* (*clasp 1* and *clasp 2*) division phenotypes during 4- to 8-cell stage transition (detailed quantification in Figure S5).

(B) Simulated MT arrays on *clasp* 2-cell template of 4-cell stage, reconstructed by merging the corresponding 8-cell daughter cell pair. Simulations were performed with edge-catastrophe and enhanced MT stabilization at developmentally new cell faces, yielding two clusters of MT array orientation correctly predicting the two *clasp* division phenotypes. Cell edges colored red indicate presence of edge-catastrophes, and different color coding of the cell faces represents the degree of MT stabilization. See also Figures S3, S5, and S6.

correctly predicted the vertical orientation of the cell division plane at the 1- to 2-cell transition, although, due to the high degree of cylindrical symmetry, it does so without fixing its angle around the symmetry axis of the embryo (Figure S6A for WT cell template and Figure S6B for *clasp* cell template). Notably, even in the presence of edge-catastrophe (simulated as the *clasp* mutant), the correct vertical orientation is maintained (Figure 6A for WT cell template and Figure 6B for *clasp* cell template). Moreover, with moderate edge-catastrophe, the division axis was constrained to a single specific direction, reminiscent of the true WT situation. This led us to hypothesize that CLASP is less active at the 1-cell stage than at later stages. Strikingly, when we implemented this stage-specific reduced CLASP activity without the auxin-mediated face stability rule (i.e., simulating a *bdl* mutant under this new condition), we obtained a proportion of horizontal and vertical divisions that closely matched the 18% horizontal divisions observed in the original *bdl* mutant (Figure 6C). In conclusion, auxin-mediated face stability from the 1-cell stage onward and CLASP-mediated edge-catastrophe reduction from the 2-cell stage onward can robustly and consistently recapitulate cell division orientations between the 1- and 16-cell stage in WT and *bdl* embryos and between the 1- and 8-cell stage in *clasp* embryos.

It is important to note that our quantification of the observed variation in the simulated CMA orientation (Figure 7) confirms the experimentally observed variation in division plane orientation in other cell types where PPB formation had been disturbed using *trm*678 mutant, i.e., in epidermis, cortex, and endodermis [15]. Finally, we noted that, under these rules, only a fraction of division predictions for the 8- to 16-cell transition of *clasp* mutants was correct. To assess this discrepancy, we looked at the growth rates of cells at this stage, inferred from the calculated cell volume increases between cell stages (Figures S6D and S6E). We observed that the correctness of prediction negatively correlated with the growth rates of cell volume. When, instead of using a re-created mother cell of the 4-cell stage embryo (by merging the corresponding daughter cell pair from 8-cell stage and hence *after* growth), we simulated MT dynamics on a true single cell of the 4-cell stage (hence, *before* growth), the prediction of cell division plane orientation correlated better with the experimentally observed ones (Figure S6C). This result indicated that, in *clasp* mutants, post-division cell growth skews our division orientation predictions. Therefore, tissue growth rates define an upper bound, above which the rules here described cannot be directly validated based on post-division cell shapes in the absence of additional growth data. This leaves open the interesting question whether mechanisms that influence MT stability depending on direction of growth-induced mechanical stress may become dominant factors in CMA orientation [41].

DISCUSSION

Here, we used a modeling framework on actual cell surface shapes and combined this with high-resolution imaging of both cell outline and MTs to derive a plausible model that recovers the orientation of formative cell divisions in the *Arabidopsis* embryo from first principles on a molecular basis. When comparing predictions of division plane orientation based on basic MT-MT interaction rules and edge-catastrophe with the predictions of the heuristic geometrical rules, it is striking that our minimal set of rules that couple intrinsic MT dynamics to the local and global geometry of the cell are by themselves already sufficient to correctly predict divisions in auxin-insensitive *bdl* cells (Figure S7). The difference between *bdl* and WT division patterns indicates that, in addition, auxin-mediated regulation is crucial to establish the WT division pattern in *Arabidopsis* embryos. In order to explain the orientation of cell division up to the 16-cell stage of WT, we parsimoniously implemented, besides the basic MT dynamics, two other factors influencing MT stability that are under biological control.

The first biological control mechanism is an auxin-dependent face stability rule, derived from our observed MT patterns on *bdl* mutant cells. The assumption that transient cortical MT stability is most strongly associated with new cell walls is not without precedence. Several observations indicate that peripheral marks instrumental for cell division orientation can transiently accumulate at specific cell faces in different organisms. In plants, *Arabidopsis* BASL marks are positioned away from

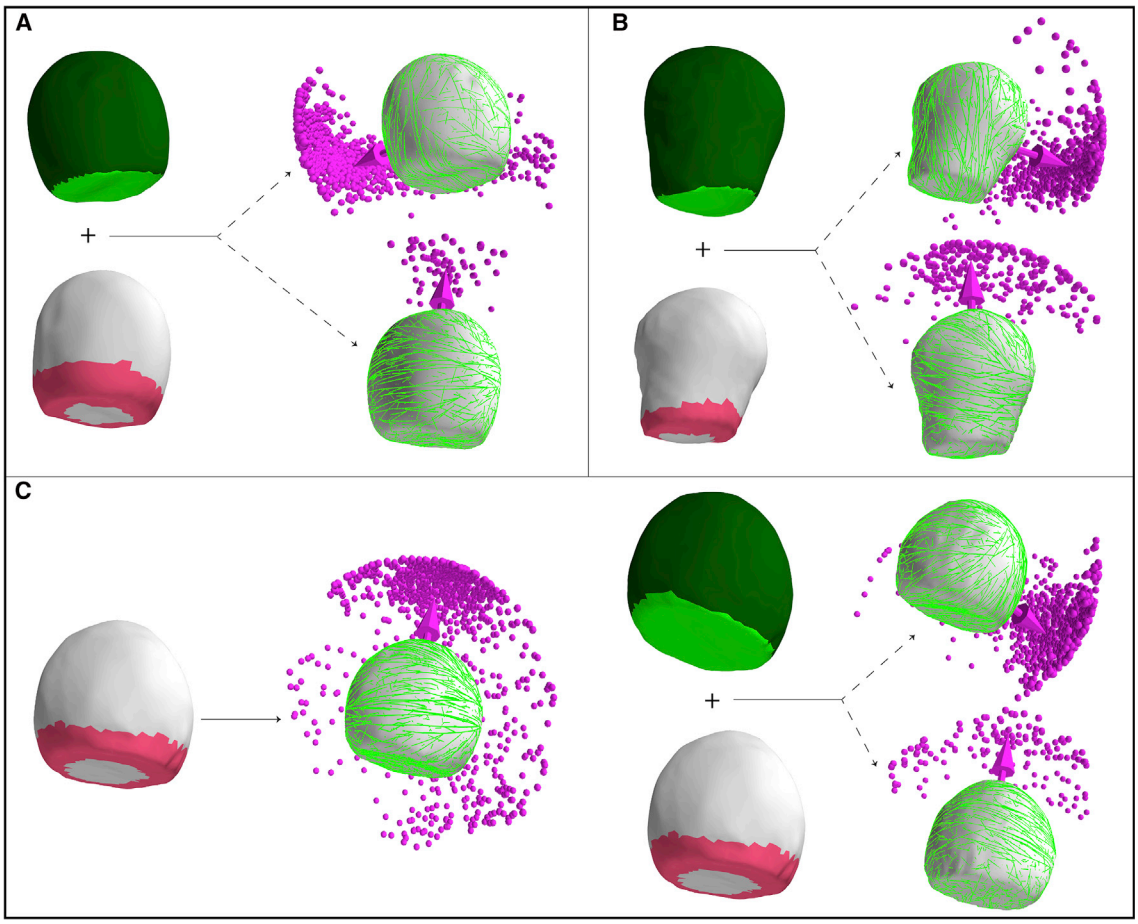

Figure 6. Fine-Tuning of the 1- to 2-Cell Stage WT, *clasp*, and *bdl* Division Patterns in *Arabidopsis* Early Embryos

(A) Simulations on WT cell template with reduced edge-catastrophe in MT dynamics and enhanced MT stabilization at developmentally new cell faces, showing a large cluster of a unique vertical MT array orientation (≈92%) that matched with the WT division plane orientation (top). A sparse cluster of horizontal MT array orientation (≈8%) was also observed (bottom).

(B) Simulations on the clasp (*clasp* 2) cell template combining reduced edge-catastrophe and enhanced MT stabilization at developmentally new cell faces showed a majority cluster of vertical MT array orientations (≈75%) matching the *clasp* division plane orientation (top) and a sparse cluster of horizontal MT array orientations (≈25%), indicating stochasticity in division plane orientation under genetic perturbation (bottom).

(C) Simulations on the *bdl* cell template with reduced edge-catastrophe resulted in a dominant horizontal orientation of MT array recapitulating the observed fraction (≈18%) of horizontal division plane orientation (left). Combination of reduced edge-catastrophe and enhanced MT stabilization at developmentally new cell faces produced a large cluster of MT array orientation (≈80%), which reflects the experimentally observed major vertical and unique division plane orientation (right, top) observed in *bdl* mutant. The remaining horizontal arrays (≈20%) indicate possible stochasticity in division plane orientation (right, bottom) under genetic perturbation, as actually observed and quantified [26]. Pink edges indicate reduced edge-catastrophes, and color coding of the cell faces represents the degree of MT stabilization.

See also Figures S3 and S6.

the previous division wall [42]. In yeast, Bud8p and Bud9p proteins mark opposite division sites during bipolar budding [43]. In order to assess to what extent this hypothesis leads to a robust mechanism, we have performed an extensive, and computationally intensive, parameter analysis (see Figure S3B). This revealed that the transient stability mechanism yields consistently correct predictions over an appreciable range of parameter values.

The second biological control mechanism is a CLASP-dependent edge-catastrophe reduction rule, based on published analyses of MTs at cell edges [17] and our own analysis of division planes in *clasp* mutant embryos. CLASP-like proteins in mammalian cells provide resistance to MTs under traction [44], and it is therefore conceivable that plant CLASPs in similar ways stabilize MT under torsion. Our parameter analysis (Figure S3A) indicates that, in contrast to the auxin-based mechanism, the activity of CLASP must be tightly regulated in order to achieve the correct divisions. It will therefore be interesting to investigate whether mutations in transcription factors that specifically change early embryo division patterns, such as BDL [1] and WOX2 [45], can be explained by their transcriptional control of MT regulators.

Our results clearly only provide evidence for sufficiency of the proposed rules and, hence, at most arguments for their plausibility. However, the fact that we were able to obtain these results without invoking other likely mechanisms, such as the role of

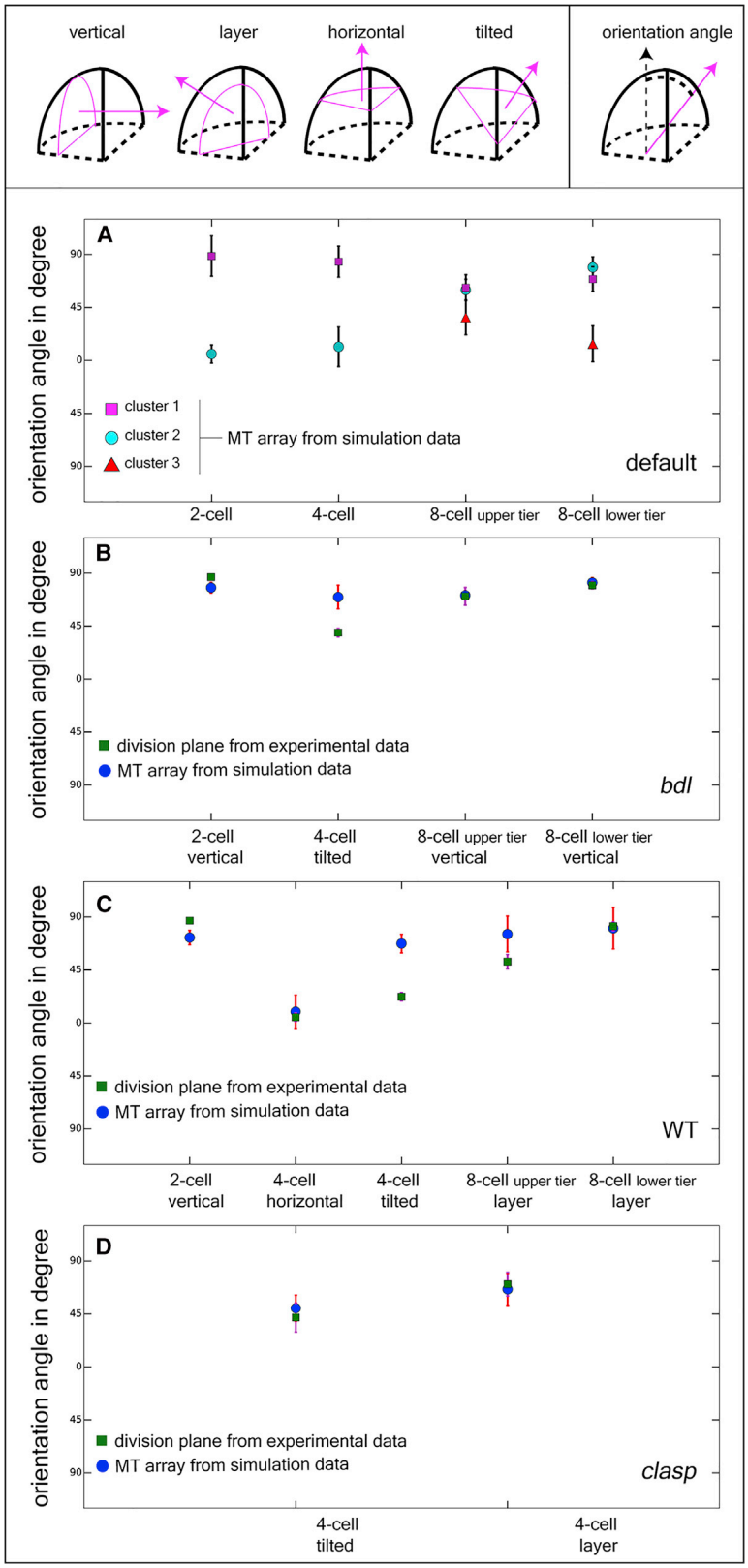

Figure 7. Comparison of Division Plane Orientation (Measured on the Basis of Experimental Data on Division Phenotype) and MT-Array Orientation (Measured on the Basis of Simulation Data)

Cell faces are classified in two types: inner faces (flat faces) and outer face (curved face). The basal face is bordered in dashed line, as this face will serve the reference for quantifying the division orientation. Different orientations are classified in four categories: (1) vertical—a plane perpendicular to the basal face and intersects the outer curved face; (2) layer—a plane perpendicular to the basal face but does not intersect the outer curved face; (3) horizontal—a plane parallel to the basal face and intersects the outer curved face; and (4) tilted—a plane other than the horizontal, vertical, and layer. Orientations were measured as the angle between the normal to the basal face (black dashed arrow) and the normal to the division plane for experimental case or MT-array order parameter vector for simulation case (solid magenta arrow).

(A) Simulated MT array orientation for default shape (i.e., considering basic MT-MT collision rules only) between 2- and 16-cell stage. For each cell stage, multiple clusters of MT array orientation were detected.

(B–D) Additional rules lead to convergence of the multiple clusters into a single cluster for each cell stage, which is compared with experimentally observed division phenotype: (B) *bdl* phenotype between 2- and 16-cell stage transitions; (C) WT phenotype between 2- and 16-cell stage transitions; and (D) *clasp* phenotype between the critical 4- and 8-cell stage transitions.

the direction of maximal wall stress in orienting the CMA, at the very least raises an interesting question. This holds in particular in view of the *bdl* mutant results, which required the minimal number of additional assumptions over and above the bare MT collision mechanism to recapitulate all successive division plane orientation decisions up to the 16-cell stage. If stress-dependent CMA orientation is indeed the dominant mechanism at this stage, why does the autonomous mechanism proposed here, which only requires the basic features of entrainment of MTs to the cell membrane and their usual (de)polymerization behavior to be operative, lead to essentially the same results? In our view, our findings suggest that the two mechanisms may well turn out to be synergistic. It is therefore interesting to see whether the stress-related mechanism can help in explaining the apparently systematic disagreement between predicted division plane angle and the experimentally observed one for the specific case of the 4-cell stage tilted divisions (see Figure 7).

In rapidly growing tissues, the sensitivity of katanin-mediated MT severing to tensile stress has been proposed as an additional array-orienting mechanism [46, 47]. This may explain the preferred orientation of cell division planes transverse to the main direction of growth in meristems, and potentially in later stage embryos, where most divisions are also oriented orthogonal to the main growth axes. It is a striking observation that our minimal model appears to be no longer sufficient exactly for the fastest growing cells, i.e., the 8- to 16-cell stage in the *clasp* mutant. Although explicit molecular hypotheses explaining katanin-mediated effects on array orientation have yet to be formulated, the local modulation of severing activity can be readily implemented within our framework [35].

Finally, it should be noted that our model is cell autonomous and does not incorporate any explicit feedback control. It essentially implements an open-ended sequence; mother cell shape dictates CMA orientation, which determines division plane orientation, which determines daughter cell shape. However, there is evidence that MT ordering contributes, through its relation with the cell wall synthesis machinery, to the anisotropy of plant cell growth [47, 48]. This suggests that a coupling of shape-dependent and tension-dependent MT organization to cell growth may create both intracellular and multicellular pathways for feedback, with changes in cell shape feeding back on the MT localization process.

In summary, our work provides a plausible theoretical framework for fundamental understanding of formative cell divisions in plants, which are not restricted to embryogenesis but continuously occur in stem cell niches where tissue growth is reduced compared to surrounding zones (e.g., [2]). Live-cell imaging methods for *Arabidopsis* embryogenesis have recently been established [49, 50]. Our model makes clear predictions on the key effects of auxin signaling and CLASP protein in specific cell faces and edges of the embryo and by extension other slow-growing cells, such as those in stem cells niches. It will now be a challenge to further develop high-resolution live imaging of the CMA in these cells in order to test the proposed molecular control mechanisms.

We envision that a combination of the basic rules of CMA organization presented here, supplemented by moderating rules involving the mechanics of wall tension and growth, may ultimately provide a complete picture of cell division control in plants and potentially the means to modify these divisions for agricultural purposes.

STAR★METHODS

Detailed methods are provided in the online version of this paper and include the following:

- KEY RESOURCES TABLE
- CONTACT FOR REAGENT AND RESOURCE SHARING
- EXPERIMENTAL MODEL AND SUBJECT DETAILS
- METHOD DETAILS
  - 3D stacks
  - cortical MT
  - Measurement of cytosolic mGFP: TUA6 signal in individual cells
- QUANTIFICATION AND STATISTICAL ANALYSIS

SUPPLEMENTAL INFORMATION

Supplemental Information includes seven figures and can be found with this article online at https://doi.org/10.1016/j.cub.2018.07.025.

ACKNOWLEDGMENTS

We thank Thomas Laux and Martin Hülskamp for critical reading of an earlier version of the manuscript. The work of B.C. was supported by a Wageningen University Graduate School grant. The work of B.M. is part of the research program of the Netherlands Organisation for Scientific Research (NWO). Simulations were carried out on the Dutch national e-infrastructure with support of the SURF Foundation.

AUTHOR CONTRIBUTIONS

B.C. developed the computational framework and performed the simulations. B.S. and B.M. developed the questions and conceptual approach underlying the study. V.W. produced 3D stacks for WT and *clasp* and analyzed cell division phenotypes. T.d.Z. and C.-Y.L. produced 3D stacks of *bdl* embryos; performed MT imaging in WT and *bdl*; and analyzed the relation between MT, PPB, and cell division orientation. B.C., V.W., T.d.Z., C.-Y.L., D.W., B.M., and B.S. wrote the paper.

DECLARATION OF INTERESTS

The authors declare no competing interests.

Received: February 23, 2018
Revised: May 18, 2018
Accepted: July 9, 2018
Published: September 20, 2018

REFERENCES

1. Yoshida, S., Barbier de Reuille, P., Lane, B., Bassel, G.W., Prusinkiewicz, P., Smith, R.S., and Weijers, D. (2014). Genetic control of plant development by overriding a geometric division rule. Dev. Cell *29*, 75–87.
2. Grandjean, O., Vernoux, T., Laufs, P., Belcram, K., Mizukami, Y., and Traas, J. (2004). In vivo analysis of cell division, cell growth, and differentiation at the shoot apical meristem in Arabidopsis. Plant Cell *16*, 74–87.
3. Campilho, A., Garcia, B., Toorn, H.V., Wijk, H.V., Campilho, A., and Scheres, B. (2006). Time-lapse analysis of stem-cell divisions in the Arabidopsis thaliana root meristem. Plant J. *48*, 619–627.
4. Hofmeister, W. (1868). Allgemeine Morphologie der Gewächse (Engelmann).

5. Sachs, J. (1878). Über die anordnung der zellen in jüngsten pflanzentheilen. Arb. des Bot. Instituts Würzbg. *2*, 46–104.
6. Errera, L. (1886). Sur une condition fondamentale d'équilibre des cellules vivantes. C. R. Hebd. Seances Acad. Sci. *103*, 822–824.
7. Besson, S., and Dumais, J. (2011). Universal rule for the symmetric division of plant cells. Proc. Natl. Acad. Sci. USA *108*, 6294–6299.
8. Smith, R.S., Guyomarc'h, S., Mandel, T., Reinhardt, D., Kuhlemeier, C., and Prusinkiewicz, P. (2006). A plausible model of phyllotaxis. Proc. Natl. Acad. Sci. USA *103*, 1301–1306.
9. Dupuy, L., Mackenzie, J., and Haseloff, J. (2010). Coordination of plant cell division and expansion in a simple morphogenetic system. Proc. Natl. Acad. Sci. USA *107*, 2711–2716.
10. Wasteneys, G.O. (2002). Microtubule organization in the green kingdom: chaos or self-order? J. Cell Sci. *115*, 1345–1354.
11. Ehrhardt, D.W., and Shaw, S.L. (2006). Microtubule dynamics and organization in the plant cortical array. Annu. Rev. Plant Biol. *57*, 859–875.
12. Mineyuki, Y. (1999). The preprophase band of microtubules: its function as a cytokinetic apparatus in higher plants. Int. Rev. Cytol. *187*, 1–49.
13. Müller, S., Wright, A.J., and Smith, L.G. (2009). Division plane control in plants: new players in the band. Trends Cell Biol. *19*, 180–188.
14. Oud, J.L., and Nanninga, N. (1992). Cell shape, chromosome orientation and the position of the plane of division in Vicia faba root cortex cells. J. Cell Sci. *103*, 847–855.
15. Schaefer, E., Belcram, K., Uyttewaal, M., Duroc, Y., Goussot, M., Legland, D., Laruelle, E., de Tauzia-Moreau, M.-L., Pastuglia, M., and Bouchez, D. (2017). The preprophase band of microtubules controls the robustness of division orientation in plants. Science *356*, 186–189.
16. Dixit, R., and Cyr, R. (2004). Encounters between dynamic cortical microtubules promote ordering of the cortical array through angle-dependent modifications of microtubule behavior. Plant Cell *16*, 3274–3284.
17. Ambrose, C., Allard, J.F., Cytrynbaum, E.N., and Wasteneys, G.O. (2011). A CLASP-modulated cell edge barrier mechanism drives cell-wide cortical microtubule organization in Arabidopsis. Nat. Commun. *2*, 430.
18. Louveaux, M., Julien, J.-D., Mirabet, V., Boudaoud, A., and Hamant, O. (2016). Cell division plane orientation based on tensile stress in *Arabidopsis thaliana*. Proc. Natl. Acad. Sci. USA *113*, E4294–E4303.
19. Zhang, Q., Fishel, E., Bertroche, T., and Dixit, R. (2013). Microtubule severing at crossover sites by katanin generates ordered cortical microtubule arrays in Arabidopsis. Curr. Biol. *23*, 2191–2195.
20. Paredez, A.R., Somerville, C.R., and Ehrhardt, D.W. (2006). Visualization of cellulose synthase demonstrates functional association with microtubules. Science *312*, 1491–1495.
21. Lloyd, C., and Chan, J. (2004). Microtubules and the shape of plants to come. Nat. Rev. Mol. Cell Biol. *5*, 13–22.
22. Hejnowicz, Z. (1984). Trajectories of principal directions of growth, natural coordinate system in growing plant organ. Acta Soc. Bot. Pol. *53*, 29–42.
23. Chakrabortty, B., Blilou, I., Scheres, B., and Mulder, B.M. (2018). A computational framework for cortical microtubule dynamics in realistically shaped plant cells. PLoS Comput. Biol. *14*, e1005959.
24. Mansfield, S.G., and Briarty, L.G. (1991). Early embryogenesis in *Arabidopsis thaliana*. II. The developing embryo. Can. J. Bot. *69*, 461–476.
25. Jürgens, G., Mayer, U., Torres Ruiz, R.A., Berleth, T., and Miséra, S. (1991). Genetic analysis of pattern formation in the *Arabidopsis* embryo. Development *113*, 27–38.
26. Scheres, B., Wolkenfelt, H., Willemsen, V., Terlouw, M., Lawson, E., Dean, C., and Weisbeek, P. (1994). Embryonic origin of the Arabidopsis primary root and root meristem initials. Development *120*, 2475–2487.
27. Liao, C.-Y., and Weijers, D. (2018). A toolkit for studying cellular reorganization during early embryogenesis in *Arabidopsis thaliana*. Plant J. *93*, 963–976.
28. Cleary, A.L., Gunning, B.E.S., Wasteneys, G.O., and Hepler, P.K. (1992). Microtubule and F-actin dynamics at the division site in living Tradescantia stamen hair cells. J. Cell Sci. *103*, 977–988.
29. Gomez, J.M., Chumakova, L., Bulgakova, N.A., and Brown, N.H. (2016). Microtubule organization is determined by the shape of epithelial cells. Nat. Commun. *7*, 13172.
30. Barbier de Reuille, P., Routier-Kierzkowska, A.-L., Kierzkowski, D., Bassel, G.W., Schüpbach, T., Tauriello, G., Bajpai, N., Strauss, S., Weber, A., Kiss, A., et al. (2015). MorphoGraphX: A platform for quantifying morphogenesis in 4D. eLife *4*, 05864.
31. Tindemans, S.H., Hawkins, R.J., and Mulder, B.M. (2010). Survival of the aligned: ordering of the plant cortical microtubule array. Phys. Rev. Lett. *104*, 058103.
32. Tindemans, S.H., Deinum, E.E., Lindeboom, J.J., and Mulder, B.M. (2014). Efficient event-driven simulations shed new light on microtubule organization in the plant cortical array. Front. Phys. *2*, 19.
33. Mitchison, T., and Kirschner, M. (1984). Dynamic instability of microtubule growth. Nature *312*, 237–242.
34. Chan, J., Sambade, A., Calder, G., and Lloyd, C. (2009). Arabidopsis cortical microtubules are initiated along, as well as branching from, existing microtubules. Plant Cell *21*, 2298–2306.
35. Deinum, E.E., Tindemans, S.H., Lindeboom, J.J., and Mulder, B.M. (2017). How selective severing by katanin promotes order in the plant cortical microtubule array. Proc. Natl. Acad. Sci. USA *114*, 6942–6947.
36. Deinum, E.E., Tindemans, S.H., and Mulder, B.M. (2011). Taking directions: the role of microtubule-bound nucleation in the self-organization of the plant cortical array. Phys. Biol. *8*, 056002.
37. Deinum, E.E., and Mulder, B.M. (2013). Modelling the role of microtubules in plant cell morphology. Curr. Opin. Plant Biol. *16*, 688–692.
38. Mirabet, V., Krupinski, P., Hamant, O., Meyerowitz, E.M., Jönsson, H., and Boudaoud, A. (2018). The self-organization of plant microtubules inside the cell volume yields their cortical localization, stable alignment, and sensitivity to external cues. PLoS Comput. Biol. *14*, e1006011.
39. Hawkins, R.J., Tindemans, S.H., and Mulder, B.M. (2010). Model for the orientational ordering of the plant microtubule cortical array. Phys. Rev. E Stat. Nonlin. Soft Matter Phys. *82*, 011911.
40. Hamann, T., Mayer, U., and Jürgens, G. (1999). The auxin-insensitive bodenlos mutation affects primary root formation and apical-basal patterning in the Arabidopsis embryo. Development *126*, 1387–1395.
41. Hamant, O., and Traas, J. (2010). The mechanics behind plant development. New Phytol. *185*, 369–385.
42. Robinson, S., Barbier de Reuille, P., Chan, J., Bergmann, D., Prusinkiewicz, P., and Coen, E. (2011). Generation of spatial patterns through cell polarity switching. Science *333*, 1436–1440.
43. Harkins, H.A., Pagé, N., Schenkman, L.R., De Virgilio, C., Shaw, S., Bussey, H., and Pringle, J.R. (2001). Bud8p and Bud9p, proteins that may mark the sites for bipolar budding in yeast. Mol. Biol. Cell *12*, 2497–2518.
44. Logarinho, E., Maffini, S., Barisic, M., Marques, A., Toso, A., Meraldi, P., and Maiato, H. (2012). CLASPs prevent irreversible multipolarity by ensuring spindle-pole resistance to traction forces during chromosome alignment. Nat. Cell Biol. *14*, 295–303.
45. Breuninger, H., Rikirsch, E., Hermann, M., Ueda, M., and Laux, T. (2008). Differential expression of WOX genes mediates apical-basal axis formation in the Arabidopsis embryo. Dev. Cell *14*, 867–876.
46. Hamant, O., Heisler, M.G., Jönsson, H., Krupinski, P., Uyttewaal, M., Bokov, P., Corson, F., Sahlin, P., Boudaoud, A., Meyerowitz, E.M., et al. (2008). Developmental patterning by mechanical signals in Arabidopsis. Science *322*, 1650–1655.
47. Uyttewaal, M., Burian, A., Alim, K., Landrein, B., Borowska-Wykręt, D., Dedieu, A., Peaucelle, A., Ludynia, M., Traas, J., Boudaoud, A., et al. (2012). Mechanical stress acts via katanin to amplify differences in growth rate between adjacent cells in Arabidopsis. Cell *149*, 439–451.
48. Paradez, A., Wright, A., and Ehrhardt, D.W. (2006). Microtubule cortical array organization and plant cell morphogenesis. Curr. Opin. Plant Biol. *9*, 571–578.

49. Gooh, K., Ueda, M., Aruga, K., Park, J., Arata, H., Higashiyama, T., and Kurihara, D. (2015). Live-cell imaging and optical manipulation of Arabidopsis early embryogenesis. Dev. Cell *34*, 242–251.

50. Kurihara, D., Kimata, Y., Higashiyama, T., and Ueda, M. (2017). In vitro ovule cultivation for live-cell imaging of zygote polarization and embryo patterning in Arabidopsis thaliana. J. Vis. Exp. e55975.

51. Weijers, D., Van Hamburg, J.-P., Van Rijn, E., Hooykaas, P.J.J., and Offringa, R. (2003). Diphtheria toxin-mediated cell ablation reveals interregional communication during Arabidopsis seed development. Plant Physiol. *133*, 1882–1892.

52. Weijers, D., Schlereth, A., Ehrismann, J.S., Schwank, G., Kientz, M., and Jürgens, G. (2006). Auxin triggers transient local signaling for cell specification in Arabidopsis embryogenesis. Dev. Cell *10*, 265–270.

53. Ambrose, J.C., Shoji, T., Kotzer, A.M., Pighin, J.A., and Wasteneys, G.O. (2007). The Arabidopsis CLASP gene encodes a microtubule-associated protein involved in cell expansion and division. Plant Cell *19*, 2763–2775.

54. Musielak, T.J., Schenkel, L., Kolb, M., Henschen, A., and Bayer, M. (2015). A simple and versatile cell wall staining protocol to study plant reproduction. Plant Reprod. *28*, 161–169.

STAR★METHODS

KEY RESOURCES TABLE

REAGENT or RESOURCE	SOURCE	IDENTIFIER
Biological Samples		
Col-0	This Lab	N/A
clasp 1	This Lab	SALK_120061
clasp 2	This Lab	SALK_83034
pWOX2:: TUA6-GFP	This Lab	ACE-W15
Chemicals, Peptides, and Recombinant Proteins		
SCRI Renaissance Stain 2200	Renaissance Chemicals	http://www.renchem.co.uk/index.php/specialty-chemicals-division/item/48-selected-fluorescent-dyes-and-brighteners-for-microscopists
Software and Algorithms		
Simulation code	custom made C++ code	available on request
Simulation analyzing code	custom made python scripts	available on request
MorphoGrapX	freely available	http://www.mpipz.mpg.de/MorphoGraphX
meshLab	freely available	http://www.meshlab.net/

CONTACT FOR REAGENT AND RESOURCE SHARING

Further information and requests for resources and reagents should be directed and will be fulfilled by the Lead Contact, Ben Scheres (ben.scheres@wur.nl).

EXPERIMENTAL MODEL AND SUBJECT DETAILS

Arabidopsis seeds were surface-sterilized and dried seeds were subsequently sown on half-strength Murashige and Skoog (MS) medium. After a 48 hour cold treatment at 4°C without light, seedlings were grown at 22°C in standard long-day (16:8 h light:dark) growth conditions. After two weeks of growth, seedlings were transferred to soil and further grown under the same conditions. Siliques were harvested from mature plants for imaging. pRPS5A>>bdl embryos were generated by pollination of homozygous RPS5A-GAL4 pistils [51] with homozygous UAS-bdl [52] pollen. For *bdl* mutant MT-imaging, pWOX2::TUA6-GFP was transformed into the RPS5A-GAL4 line. Homozygous RPS5A-GAL4 X pWOX2::TUA6-GFP pistils were subsequently pollinated using either Col-0 or UAS-bdl.

METHOD DETAILS

3D stacks

Arabidopsis ovules of Col-0, *clasp 1* and *clasp 2* have been isolated from siliques in SCRI Renaissance 2200 solution on an objective slide [53, 54]. The embryos have been popped out of the ovules by applying gentle pressure on the coverslip. 3D stacks of the embryos have been made using of Zeiss LSM710 with the 405nm laser. For generating 3D stacks of *bdl* embryos, images were collected on a Leica SP5 confocal laser scanning microscope after staining according to [1].

cortical MT

Arabidopsis siliques were cut open using a fine needle and ovules were mounted and stained in a MT imaging solution (10% glucose, 10 uM Taxol, 0.1 M Pipes, pH 6.8, 1 mM EGTA, 1 mM MgSO4) containing 0.1% Renaissance (SR2200; Renaissance Chemicals; stock solution of the supplier was considered as 100%) cell wall counter-stain. Embryos were separated from ovules by gently pressing the coverslip. Images were taken within 30 minutes after release from the ovule. Sequential images were taken with 0.2 μm intervals to create high-resolution Z stacks. Images were obtained using the Leica SP5 confocal laser scanning microscope equipped with photon-counting HyD detector and x63 water immersion objective. GFP and SR2200 signals were detected at 488nm excitation/500-530nm emission or 405nm excitation/520-560nm emission wavelength, respectively.

Measurement of cytosolic mGFP: TUA6 signal in individual cells

The optical section containing the great circle of the nucleus was visually defined, a maximum projection containing 5 optical sections, 2 above, 2 beneath the optical section with the great circle, and the optical section containing the great circle, was then generated from the raw image stack. A 0.2 to 0.4 μm^2 region of interest (ROI) in the cell of interest was given at where no distinguishable

microtubule structure was found. The average mGFP fluorescence signal intensity in this ROI was documented and defined as the cytosolic mGFP: TUA6 signal of the cell of interest. The difference in average cytosolic mGFP: TUA6 signals were tested via two-tailed Student's t test with MS Excel.

QUANTIFICATION AND STATISTICAL ANALYSIS

Cell segmentation and cortical MT projection were performed in MorphoGraphX (version 2.0) [30]. SR2200 stacks (tiff) were Guassian blurred using Sigma 0.3 μm. Blurred stacks were segmented using ITK watershed auto seeded segmentation with levels ranging from 500-1500. From segmented cells, meshes were created using Marching cubes 3D with Cube size in the range 0.5-1.0. cortical MT (pWOX2::TUA6-GFP) stacks (tiff) were loaded and overlaid with created corresponding cell meshes. Absolute cortical MT signal with a distance of 0-1 μm relative to the cell surface was projected on the cell mesh. Number of embryonic cells used in the simulations are tabulated below.

Phenotype	1-cell stage	2-cell stage	4-cell stage	8-cell stage
WT	4	4	4	4
bdl	4	4	4	4
clasp 1		2	2	
clasp 2	1	4	4	